

Full Length Article

An effective oxygen vacancy restrain method for flexible perovskite solar cells with enhanced performance and bending resistance



Yanling Tang¹, Yue Lei¹, Haiming Li^{*}, Yufeng Wu, Yunzhe Li, Shuqian Liu, Hanyu Wang, Xingchong Liu^{*}

School of New Energy and Materials, Southwest Petroleum University, Chengdu 610500, P. R. China

ARTICLE INFO

Keywords:

SnO_2
Electron transport layer
Flexible perovskite solar cells
Trichlorobenzene sulfonic acid potassium salt

ABSTRACT

Flexible perovskite solar cells (F-PSCs) are currently a research hotspot due to their lightweight, solution processability, and low cost. However, oxygen vacancies in SnO_2 would deteriorate the crystallization of perovskite, especially in F-PSCs due to the low temperature of SnO_2 preparation with flexible substrates, thus inducing poor performance and decreased bending resistance. Here, trichlorobenzene sulfonic acid potassium salt (TSAPS) is used as an effective oxygen vacancy restrain additive on the SnO_2 surface for F-PSCs. The oxygen vacancies are reduced from 68.40% to 45.26% after TSAPS modification. Meanwhile, the interfacial defects are suppressed by the synergistic passivation of individual ions in TSAPS, thus the carrier extraction and transportation are effectively improved. As a result, the PCE of the F-PSCs greatly increased from 15.22% to 18.63%. In addition, the unencapsulated SnO_2 /TSAPS-based flexible device can maintain 84% of its initial efficiency after 3000 bending cycles, exhibiting superior mechanical stability, while the control one decreased to only 9%. This work demonstrates a dependable method for improving the quality of the interface between the ETL and perovskite layer, resulting in enhanced bending resistance and performance for flexible PSCs.

1. Introduction

Flexible perovskite solar cells (F-PSCs) are suited for far too many different applications, including wearable electronics, portable energy sources, and deployable tents, due to their lightweight and bending flexibility [1–3]. Today, as gadget architectures and material processing continue to advance, the PCE of F-PSCs in the laboratory has exceeded 21% [4,5]. They show superior potential in the field of photovoltaics [6].

However, the performance of F-PSCs is limited due to the deformability of the flexible substrate which leads to interfacial residual stresses and lattice mismatch [7–9]. The thermal expansion/shrinkage of the flexible substrate during processing exacerbates this interfacial adhesion, thus presenting prominent problems in charge transportation and mechanical stability in F-PSCs [10,11]. SnO_2 was used as an optimal electron transport layer (ETL) in F-PSCs to achieve a functional layer that can be processed at low temperatures [12]. However, it still has unsatisfactory aspects such as oxygen vacancies, lattice mismatch, and overwide energy level matching with the perovskite layer [13]. In

addition, there are still physical property differences between inorganic SnO_2 and organic-containing perovskite (PVK), resulting in significant interfacial residual stresses at the SnO_2 /perovskite interface as well [12,14], thus leading to mechanical delamination [12], affecting the photovoltaic performance and mechanical durability of F-PSCs.

To solve the SnO_2 /perovskite interface problem, Mo et al. [15] used halide KBr as the modified layer to regulate the SnO_2 /perovskite interface, and the stability of F-PSCs was significantly improved, and the original efficiency of about 81% could be maintained after 1000 bending cycles. Additives such as EDTA [16] were added to the SnO_2 layer, forming a complex between SnO_2 and perovskite to promote the growth of PVK films to improve the mechanical durability of F-PSCs. Zheng et al. [17] used HCOONH_4 as an embedded layer in the ETL, with a bottom-up overall penetration process, the ETL and perovskite were both modified, and thus improved the performance of F-PSCs. The investigated interfacial modification strategy can effectively inhibit the formation of interfacial defects. For instance, potassium ions (K^+) are considered representative additives to improve the PCE of SnO_2 -based planar F-PSCs by eliminating hysteresis and promoting ion migration [15]. It is

* Corresponding authors.

E-mail addresses: lucialee@126.com (H. Li), liuxc_76@163.com (X. Liu).

¹ These authors contributed equally to this work.

reported that Yi et al. [4] used a series of halides as interface layers to regulate the SnO_2 /perovskite interface, in which the device efficiency of F-PSCs reached to 18.16% and showed excellent stability. Of the four carbon-halogen bonds, the C-Cl bond has the largest dipole moment (C-Cl of 1.46, C-F of 1.41, C-Br of 1.38, and C-I of 1.19)[19,20]. Therefore, it is expected that the C-Cl bond will show a more excellent passivation effect. In addition, organic small molecules with specific functional groups, such as amines ($-\text{NH}_2$)[21], sulfonic acids ($-\text{SO}_3^-$)[22] and halides (F [22], Cl [23], etc.) as Lewis bases/acids, can be coordinated with interfacial metal atoms, which can significantly change the energy level of SnO_2 and effectively reduce surface defects [24–26]. Although a large number of studies have been reported on the surface passivation between ETL and perovskite, they have paid more attention to the interaction with uncoordinated Sn^{4+} or Pb^{2+} (such as Table S2), few reports have been mentioned about the inhibition of oxygen vacancy and the regulation of energy level for tin oxide.

In this study, trichlorobenzene sulfonic acid potassium salt (TSAPS) is used as an effective oxygen vacancy restrain additive for the SnO_2 /perovskite interface, which greatly improves the performance and

stability of F-PSCs. The interaction between TSAPS and ETL effectively reduces the surface trap states of SnO_2 films and enhances the energy level matching between ETL and PVK. Meanwhile, the synergistic passivation of Cl^- , $-\text{SO}_3^-$ and K^+ in TSAPS suppresses the interfacial defects and promotes the carrier extraction and transportation, thus significantly improving the V_{oc} and FF . The results show that the performance of SnO_2 /TSAPS-based flexible PSCs is significantly boosted, with PCE increased from 15.22% to 18.63% and hysteresis decreased from 11% to 4%. In addition, the unencapsulated device of the SnO_2 /TSAPS-based flexible PSC exhibits good mechanical stability under 3000 bending cycles, which can maintain 84% of its initial efficiency, while the control one can only keep 9%.

2. Results and discussion

TSAPS molecules with multiple functional groups are used to modify the SnO_2 /perovskite interface. The chemical structure of TSAPS and details of the preparation process of the perovskite solar cells are shown in Fig. S1 (Supporting Information). The structure diagram of TSAPS is

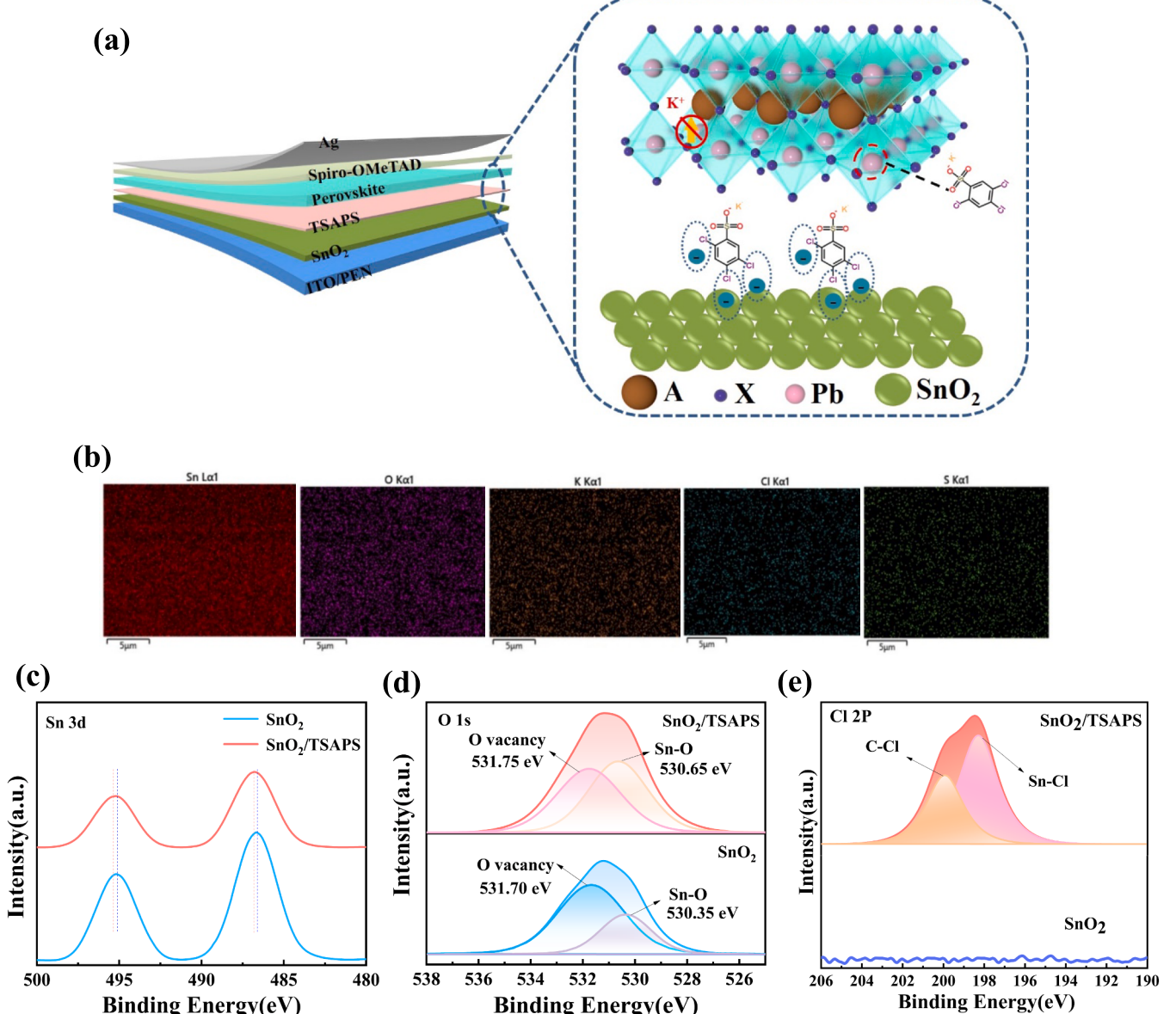


Fig. 1. (a)Structure of PSCs and the interaction mechanism of TSAPS molecule with the device at SnO_2 /perovskite interface. (b)EDS results of Sn, O, K, Cl and S of FTO/ SnO_2 -TSAPS film. (c) Sn 3d, (d) O 1 s, and (e) Cl 2p XPS spectra of the original and TSAPS modified SnO_2 films.

shown in Fig. S1a, which contains C-Cl bonds in TSAPS as well as sulfonic acid groups and K^+ that can deactivate deep defects in perovskite films. The electron-rich C-Cl bond can interact with uncoordinated Sn^{4+} to restrain oxygen vacancy on the surface of tin oxide and promote carrier transport [27]. Meanwhile, sulfonate ions are expected to passivate uncoordinated Pb^{2+} in perovskite films, thereby inhibiting non-radiative recombination [28]. In addition, K^+ can enter the perovskite film to reduce hysteresis [15]. The interaction mechanism of the TSAPS molecule with the F-PSCs at SnO_2 /perovskite interface is displayed in Fig. 1a, with the device structure of PEN-ITO/ SnO_2 /TSAPS/ $Cs_{0.05}(FA_{0.85}MA_{0.15})_{0.95}Pb(I_{0.8}Br_{0.15}Cl_{0.1})_3$ /Spiro-OMeATD/Ag. F-PSCs based on $Cs_{0.05}(FA_{0.85}MA_{0.15})_{0.95}Pb(I_{0.8}Br_{0.15}Cl_{0.1})_3$ demonstrate superior mechanical bending durability compared to conventional flexible perovskite material ($FAPbI_3$)_{1-x}($MAPbBr_3$)_x.

There are many O vacancies and Sn interstitial defects in SnO_2 , which would act as recombination centers and traps, leading to decreased carrier collection and transportation, thus potassium trichlorobenzene sulfonate (TSAPS) was introduced between SnO_2 and perovskite layer to reduce defects, carrier recombination, and hysteresis by using the synergistic effects of its organic anions and potassium ions [12]. To verify the interaction between TSAPS and tin oxide, we tested the energy dispersive spectrometer (EDS) of the original and modified tin oxide films. As shown in Fig. 1b, the EDS images reveal the morphology of the films before and after TSAPS modification. S, Cl and K elements can be detected on the surface of the SnO_2 /TSAPS thin film, proving the presence of TSAPS at the SnO_2 interface. Meanwhile, compared with a full spectrum of SnO_2 , the same three elements of S, Cl, and K appear in the XPS spectrum of the modified film (Fig. S2, Supporting Information), further confirming the presence of TSAPS on the surface of SnO_2 .

Fig. 1c shows the Sn 3d XPS results, it can be seen that the peaks of $Sn\ 3d_{3/2}$ and $Sn\ 3d_{5/2}$ are redshifted about 0.3 eV relative to SnO_2 , revealing the presence of a small number of negatively charged particles around the Sn atoms [21,29], the negative charges around Sn presumably results from the highly electronegative coupling with Cl atom at 198.15 eV, forming an Sn-Cl bond [17] (Fig. 1e), confirming that when TSAPS is deposited on the surface of SnO_2 , the interaction between Cl^-

and Sn^{4+} occurs due to the difference of the electronegativity [30].

Based on further analyzing the spectrum of O1s (Fig. 1d), we found that asymmetric wide peaks exist, which can be deconvolved into two narrow peaks. the peak of the Sn-O bond of the original SnO_2 appears at 530.35 eV, due to the absorbed hydroxyl group on the surface [23,31], another peak at 531.70 eV related to oxygen vacancy (O_v) or surface absorbed hydroxyl (O_{OH}), while the TSAPS passivation results in 530.65 eV and 531.75 eV. The peak of 530.35 eV is assigned to the lattice oxygen of SnO_2 , and the peak of 531.70 eV is assigned to the chemisorbed oxygen on the SnO_2 substrate. After TSAPS modification, the adsorbed oxygen intensity of SnO_2 is weakened, and the lattice oxygen strength is enhanced. We used origin to calculate the 531.70 eV and 531.75 eV peak area (Table S1, Supporting Information), and found that the oxygen adsorption content ($(O_v + O_{OH})/O_{all}$) in the original SnO_2 was approximately 68.40%, After TSAPS modification, the oxygen adsorption content decreased to 45.26%, meaning that TSAPS modification can fill oxygen vacancies, This may be due to the negatively charged C-Cl bond [27]. The high electronegative element Cl fascinated electrons, thus prohibited the reduction of Sn^{4+} to restrain the oxygen vacancies at the tin oxide interface, which is favorable for carrier transportation [32].

The surface morphology of the TSAPS modified SnO_2 film was further studied. AFM was characterized for SnO_2 and SnO_2 /TSAPS films (Fig. S3, Supporting Information). The root mean square (RMS) of the TSAPS-modified SnO_2 film surface is 14.0 nm compared with 17.7 nm of the original one, indicating that the morphology of the modified film does not show much difference. Kelvin probe force microscopy (KPFM) is used to study the surface potential of the substrate. In the KPFM plots of Fig. 2a and 2b, the contact potential difference (CPD) of TSAPS-modified SnO_2 (-537 mV) is lower than that of the pristine one (-269 mV), which indicates that the TSAPS-modified ETL is beneficial for extracting carriers. Fig. 2c reveals that the contact angle of SnO_2 decreased from 15.8° to 10.5° after TSAPS modification, manifesting easier deposition for the PVK layer on TSAPS/ SnO_2 surface. The decreased CPD and contact angle on the SnO_2 surface can also effectively reduce the Gibbs free energy of perovskite, thus facilitating the nucleation process [33] and enlarging the size of PVK crystals [30].

To further evaluate the change the energy level of SnO_2 , UV-vis

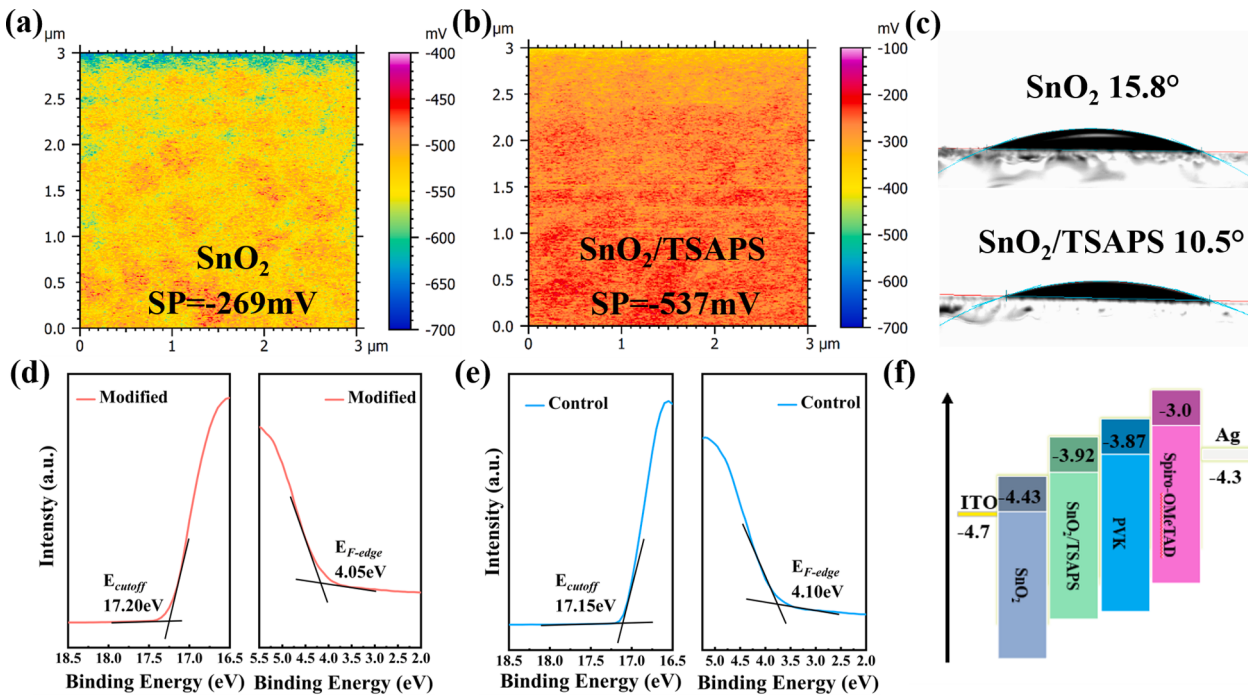


Fig. 2. KPFM results of (a) standard and TSAPS modified SnO_2 films. (c) Water contact angle of SnO_2 and SnO_2 /TSAPS films. UPS test results of (d) SnO_2 and (e) SnO_2 -TSAPS. (f)schematic illustration of the energy level.

transmittance tests and ultraviolet photoelectron spectroscopy (UPS) tests for with and without TSAPS modified SnO_2 films were characterized [34]. UV-vis transmittance tests (Fig. S4a, Supporting Information) show that the original SnO_2 film and the modified one both reveal superior light transmittance, contributing to high light absorption for perovskite. Fig. S4b, Supporting Information, demonstrates the $(\alpha h\nu)^2$ as a function of photon energy for SnO_2 film with and without TSAPS. The band-gap (E_g) of the pristine and modified SnO_2 are determined to be 3.80 eV. As shown in Fig. 2d and 2e, the Fermi edge (E_{F-edge}) and cutoff binding energy (E_{cutoff}) of SnO_2 ETL before and after TSAPS modification were 4.10, 4.05 eV and 17.15, 17.20 eV, respectively. Fermi level (E_F) of the pristine and modified SnO_2 are calculated by model $E_F = 21.22 - E_{cutoff}$ to be -4.07 eV, -4.02 eV, respectively. The valence band position (E_{VB}) of SnO_2 before and after modification are calculated to be -8.17 , -8.10 eV, respectively, by the model of $E_{VB} = E_g - E_{F-edge}$, and the conduction band positions (E_{CB}) were calculated by the model $E_{CB} = E_g + E_{VB}$ to be -4.05 , -3.92 eV. The energy level distribution of the modified devices is shown in Fig. 2f. The E_{CB} of TSAPS-modified SnO_2 is slightly increased and is closer to that of perovskite (-3.87 eV [31]). The energy level shifts indicate the presence of n-doping in SnO_2 , which lower the highest occupied molecular orbital (HOMO) energy level of SnO_2 , thus favoring energy level alignment and electron extraction [34,35]. Therefore, the TSAPS-modified SnO_2 ETL is expected to decrease interfacial energy barriers and promote the extraction of electrons, leading to the increase of device V_{OC} .

To verify the effect of the TSAPS modification on the crystallinity of the perovskite, X-ray diffraction (XRD) was performed for the original and TSAPS modified perovskite films. As shown in Fig. 3a, the characteristic diffraction peak positions of the perovskite films are essentially the same, indicating improved crystallization without changing the observable lattice parameters. The PbI_2 peak is significantly suppressed for the modified PVK film due to that the $-\text{SO}_3^-$ in TSAPS penetrates into the perovskite layer and interacts with Pb^{2+} (Fig. 3b), thereby reducing trapped defects and enhancing the crystallinity of PVK film [32,36]. Fig. S5 (Supporting Information) demonstrates the full width at half-maximum (FWHM) of the perovskite peak of the (220) plane. The

minimum FWHM appears in the 1 mg/ml TSAPS modified perovskite film. The lower the FWHM, the larger the grain size [37]. SEM images also confirmed the XRD results. Fig. 3(c-f) and Fig. S6(a-d) (Supporting Information) show the SEM images of the perovskite surface before and after TSAPS modification. It can be seen that the grain size of the perovskite film increases significantly with the introduction of the TSAPS interfacial layer, this is attributed to the interaction of $-\text{SO}_3^-$ with Pb^{2+} to delay the crystallization process of perovskite, which is conducive to obtaining high-quality perovskite films [28]. And the grain size is the largest when the concentration of TSAPS is 1 mg/ml, indicating that 1 mg/ml is the optimal concentration of TSAPS. Larger grain size means fewer grain boundaries, which is beneficial for charge transfer and collection [38,39], further confirming that TSAPS not only promotes the crystallization of PVK but also improve electron extraction. The increase of the grain size could also be conjectured by the result of ultra-violet-visible (UV-vis) spectrophotometry. In Fig. S7, (Supporting Information), $\text{SnO}_2/\text{TSAPS}$ -based perovskite film exhibits enhanced absorption intensity in the region of 300–550 nm wavelength. The enhanced absorption is likely attributed to the increase of grain size and crystallinity, which improves the collection and utilization of light due to stronger light scattering [40].

In order to further explain the influence of TSAPS on the annealing crystallization process, X-ray photoelectron spectroscopy (XPS) was used to characterize the coordination between TSAPS and perovskite. Fig. S8a demonstrates the $\text{Pb } 4f_{5/2}$ and $\text{Pb } 4f_{7/2}$ XPS peaks located at 143.55 eV and 138.7 eV for original perovskite films, which blue-shifted to 143.2 eV and 138.3 eV in the modified one, respectively, the interaction between $-\text{SO}_3^-$ and the uncoordinated Pb^{2+} was demonstrated, which helped to inhibit non-radiative recombination [28]. At the same time, the binding energy of $\text{I } 3d$ in the perovskite films shows a corresponding shift (Fig. S8b, Supporting Information), which is due to the presence of Cl^- that intensify the chemical bond between the lead and anions, thus inhibiting the ion migrations and generation of vacancies [41].

In addition, photoluminescence (PL) and time-resolved photoluminescence (TRPL) spectra of perovskite layers were used to attest the

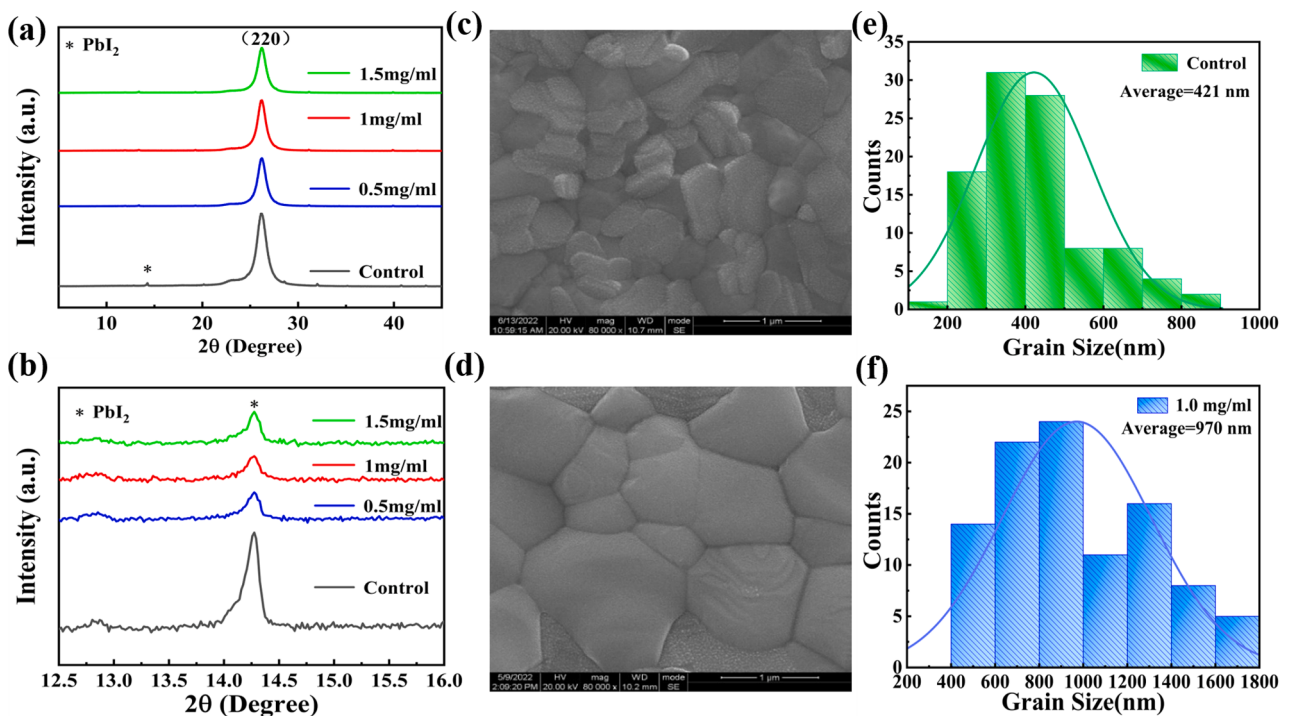


Fig. 3. (a) XRD patterns of perovskite film before and after TSAPS modification.(b) partial enlarged image of XRD. (c-f) Grain size statistics of TSAPS modified perovskite films with different concentrations.

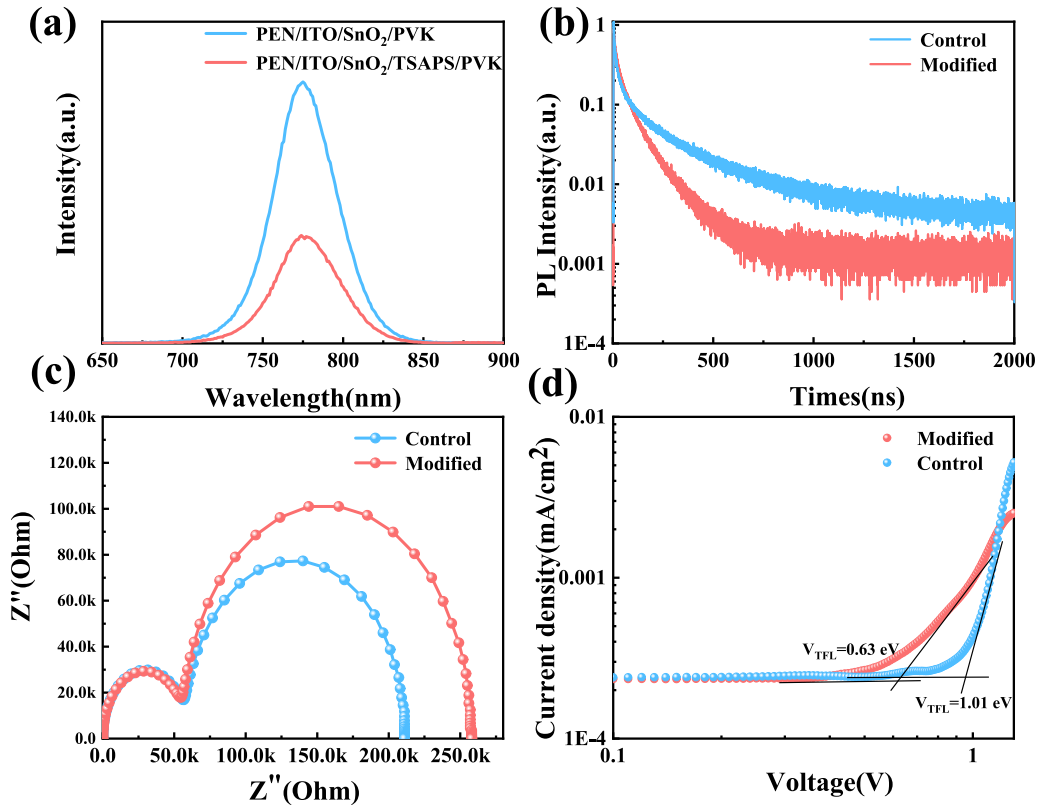


Fig. 4. (a) PL and (b)TRPL patterns of perovskite film before and after TSAPS modification. (c) EIS profiles of unmodified and optimally modified F-PSCs. (d)Dark-state J-V curves of unmodified and optimally modified F-PSCs.

reduction of the trap state density and the boost of interfacial carrier transfer in high-quality modified films. the photoluminescence (PL) intensity of the SnO₂/TSAPS-based perovskite film is significantly lowered compared to the pristine one (Fig. 4a), which indicates that the modified film has the best PL burst, suggesting that TSAPS promotes carrier migration from perovskite to ETL and the defect state density is reduced [42,43]. Also, time-resolved photoluminescence (TRPL) shows that the lifetime of SnO₂/TSAPS-based perovskite is significantly shorter compared to that of pristine one (Fig. 4b), which is consistent with the steady-state PL results. The shortened lifetime indicates a faster charge transfer from PVK to ETL after modification [42].

We analyze the effects of TSAPS modification on load transfer and composite resistance through electrochemical impedance spectroscopy (EIS). A more minor transport resistance (R_{tr}) and a larger recombination resistance (R_{rec}) can be found in perovskite devices with TSAPS addition in Fig. 4c, since the two arcs in high- frequency and low-frequency represent R_{tr} and R_{rec} , respectively [37,44]. The smaller transport resistance indicates that the device has better charge transfer capability, and the larger R_{rec} can effectively suppress non-radiative recombination, resulting in better photovoltaic performance. Similarly, Fig. 4d shows the dark-state J-V curves for only electron device with structure of PEN/ITO/SnO₂/(with or without TSAPS)/perovskite/PCBM/BCP/Ag. It can be seen from the space charge limited current (SCLC) curves that the trap-filling limit voltage (V_{TFL}) of the TSAPS-modified flexible device is reduced to 0.5 times that of the original one, which is 0.63 V and 1.01 V, respectively. The reduced V_{TFL} can be attributed to decreased defect density, carrier recombination and hysteresis that results from the synergistic effect of organic anions and potassium ions of TSAPS [45].

The J-V curves before and after the modification are shown in Fig. 5a, and the detailed parameters are shown in Table 1. Under standard sunlight (1.5 AM, 100 mW/cm²), the PCE of F-PSCs increased and then decreased with the increase of TSAPS concentration, reaching a

champion of 18.63% at a concentration of 1 mg/ml, with V_{OC} of 1.094 V, J_{SC} of 23.24 mA/ cm² and FF of 73.30%. The TSAPS-modified F-PSCs show significantly higher V_{OC} and FF than the control one, which is mainly due to the reduction of defects and carrier recombination. The increased J_{SC} of TSAPS-modified F-PSCs can be attributed to the increased particle size and enhanced charge transport capacity [46]. When the concentration of TSAPS is further increased, the efficiency of the device decreases, which is due to the excessive TSAPS residues forming impurities at the interface, hindering the carrier transportation and thus affecting the optoelectronic performance [37]. Fig. 5b shows the external quantum efficiency (EQE) of the flexible devices before and after TSAPS modification, and the integrated currents are calculated to be 22.19 mA/cm² and 23.69 mA/cm², respectively, which are consistent with the J-V results. In addition, J-V statistic results based on 20 devices are shown in Fig. S10 (Supporting Information), which proves that the modified devices have good performance repeatability.

Hysteresis responses were performed on the devices, as shown in Fig. 5c. It is found that the hysteresis index (HI) of the flexible device is reduced from 11% to 4% after TSAPS modification, which is mainly due to the existence of K⁺. K⁺ can eliminate the capture defect of the ETL/perovskite interface to improve the performance of PSC, prevent the formation of iodine Frenkel defects and suppress ion migration [47].

The stability and anti-bending properties after TSAPS modified are also greatly improved. As shown in Fig. 5d, the TSAPS-modified devices were found to have outstandingly high stability after continuous monitoring when placed in N₂ filled glove box in the dark for 50 days, maintaining 92% of its initial values, while the standard one could only keep 73%.

As a flexible device, the most critical and practical aspect is efficiency and bending stability. It can be seen from Fig. 6a and 6b that after 3000 bending cycles, the cracks in the TSAPS-modified SnO₂/perovskite film are very small, while the original one is coarse and numerous, indicating that TSAPS effectively promotes the bending resistance and greatly

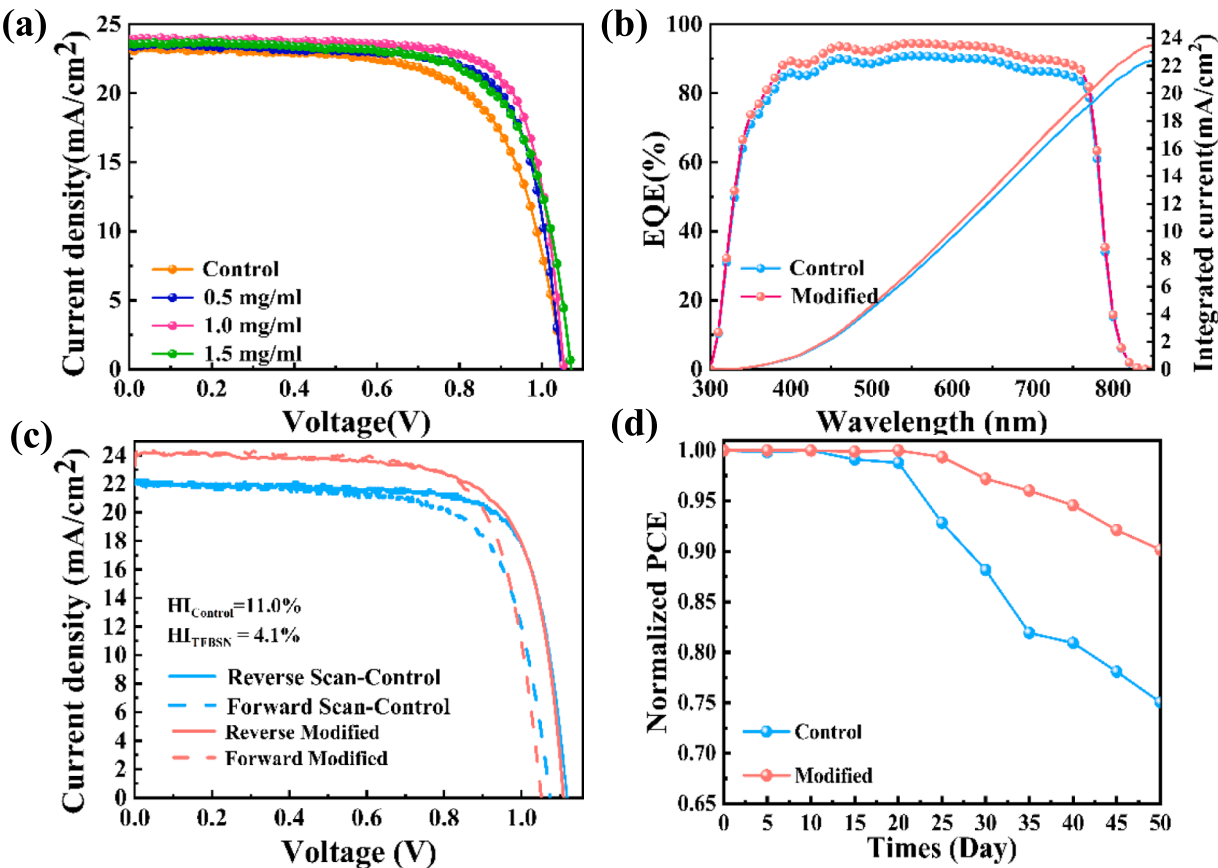


Fig. 5. (a) J - V curves of pristine and different concentrations of TSAPS-modified F-PSCs; (b) EQE and integral currents of unmodified and optimally modified F-PSCs. (c) Hysteresis curves of unmodified and optimally modified F-PSCs. (d) PCE efficiency stability of unmodified and optimally modified F-PSCs.

Table 1
Champion and average photovoltaic parameters of control and TSAPS-modified F-PSCs.

Device	V_{OC} (V) (average)	J_{SC} (mA/cm ²) (average)	FF (%) (average)	PCE (%) (average)
Control	1.022 (1.007)	23.05 (21.47)	64.60 (64.95)	15.22 (14.03)
0.5 mg/ml	1.046 (1.022)	23.63 (22.53)	74.00 (71.17)	18.28 (16.38)
1 mg/ml	1.094 (1.048)	23.24 (22.74)	73.30 (72.11)	18.63 (17.16)
1.5 mg/ml	1.071 (1.001)	23.76 (21.72)	70.30 (71.41)	17.89 (15.51)

increases the mechanical flexibility. Fig. 6d demonstrates that TSAPS-modified flexible device can maintain 84% of its initial efficiency after 3000 bending cycles while the control one sharply decreases to 9%, showing that TSAPS can validly enhance the mechanical resistance and stability of the whole device.

In addition, since the benzene ring has good hydrophobicity, the TSAPS can also promote the moisture stability of the flexible devices. Fig. S6 (Supporting Information) reveals the water contact angle of the PVK films, it can be seen that the TSAPS-modified perovskite has a larger contact angle, manifesting better hydrophobicity. Fig. 6c demonstrates that the modified device can maintain 83% of its initial efficiency after 7 days of ageing under $60\% \pm 5$ relative humidity in ambient dark conditions without any encapsulation, and the original one can only keep 52%, which is mainly due to the synergistic effect of TSAPS that induces decreased defects at the interface and grain boundaries, thus leading to enhanced device performance and moisture stability.

3. Conclusion

In summary, TSAPS interlayer between the SnO_2 and perovskite

effectively improves the performance of F-PSCs. The chemical interaction between TSAPS and ETL reduces the trap state on the surface of SnO_2 films, resulting in enhanced energy level matching between ETL and PVK. A smaller contact angle on the ETL substrate facilitates the formation of high-quality PVK films with increased grain size and effectively reduces the defect density. And interfacial defects are suppressed by the TSAPS, which optimizes the carrier extraction and transport, thus significantly improving the V_{OC} and FF . Eventually, the photovoltaic performance of the SnO_2 /TSAPS-based F-PSCs was validly improved, with a PCE of 18.63% enhanced from 15.22%, and greatly reduced hysteresis. In addition, modified F-PSCs demonstrate effectively enhanced bending resistance and moisture stability. The unencapsulated devices of the SnO_2 /TSAPS-based F-PSCs can maintain 84% of its initial efficiency after 3000 bending cycles, and retain 83% of pristine PCE after 7 days under $60\% \pm 5$ relative humidity in ambient dark condition without any encapsulation, while the control one can only maintain 9% and 52%, respectively. This work provides a reliable way to improve the quality of buried interfaces on F-PSCs for efficient and stable flexible perovskite solar cells.

CRediT authorship contribution statement

Yanling Tang: Conceptualization, Data curation, Writing – original draft. **Yue Lei:** Methodology, Data curation. **Haiming Li:** Writing – review & editing, Funding acquisition, Resources. **Yufeng Wu:** Investigation, Validation. **Yunzhe Li:** Formal analysis, Methodology. **Shuqian Liu:** Investigation, Formal analysis. **Hanyu Wang:** Investigation. **Xingchong Liu:** Writing – review & editing.

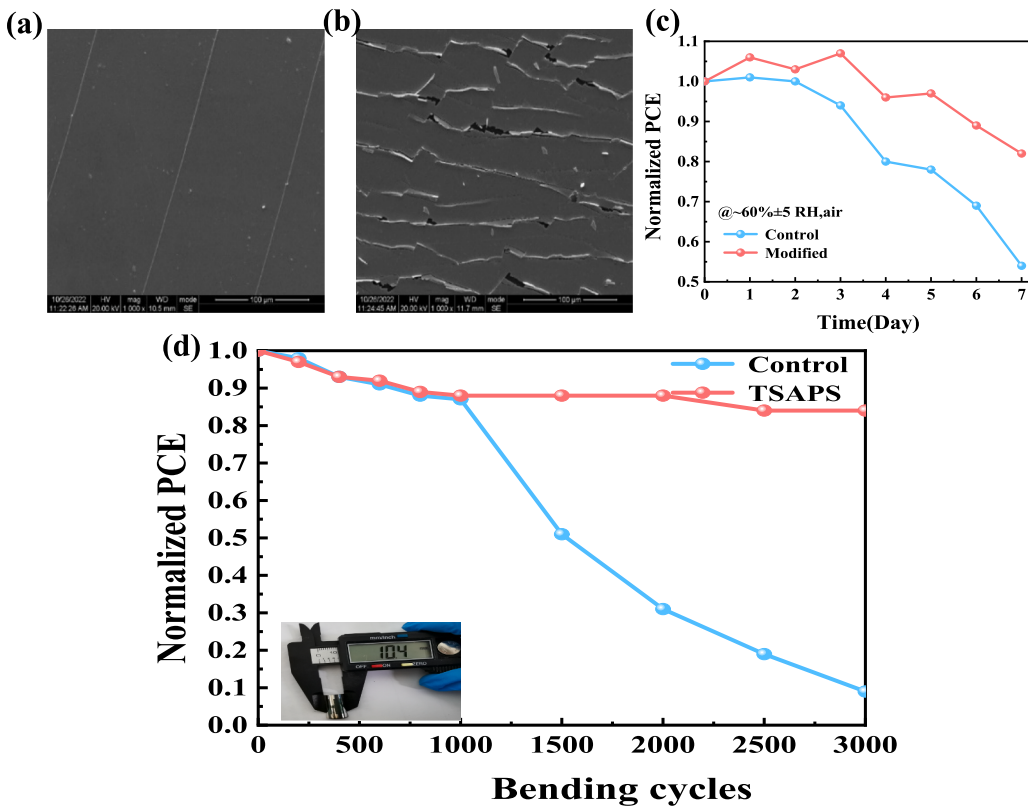


Fig. 6. Surface topography of (a) SnO₂ and (b) SnO₂/TSAPS based perovskite films. (c) moisture stability of F-PSCs. (d) PCE stability of SnO₂ and SnO₂/TSAPS based F-PSCs under 3000 bending cycles.

Declaration of Competing Interest

The authors declare that they have no known competing financial interests or personal relationships that could have appeared to influence the work reported in this paper.

Data availability

The authors do not have permission to share data.

Acknowledgements

This work was supported by the Nature Science Funds of Sichuan Province (No.2022NSFSC0266), and the Young Scholars Development Fund of SWPU (No. 201999010017).

Appendix A. Supplementary material

Supplementary data to this article can be found online at <https://doi.org/10.1016/j.apsusc.2023.158416>.

References

- [1] D.X. Du, F.Y. Qiao, Y.K. Guo, F.Y. Wang, L.N. Wang, C. Gao, D.Z. Zhang, J.J. Liang, Z.P. Xu, W.Z. Shen, H.Y. Wang, Photovoltaic performance of flexible perovskite solar cells under bending state, *Sol. Energy* 245 (2022) 146–152.
- [2] D.Y. Liu, T.L. Kelly, Perovskite solar cells with a planar heterojunction structure prepared using room-temperature solution processing techniques, *Nat. Photonics* 8 (2014) 133–138.
- [3] D.H. Shin, J.H. Heo, S.H. Im, Recent advances of flexible hybrid perovskite solar cells, *J. Korean Phys. Soc.* 71 (2017) 593–607.
- [4] Z.J. Yi, B. Xiao, X. Li, Y.B. Luo, Q.H. Jiang, J.Y. Yang, Revealing the interfacial properties of halide ions for efficient and stable flexible perovskite solar cells, *J. Colloid Interface Sci.* 628 (2022) 696–704.
- [5] D.P. Gao, B. Li, Z. Li, X. Wu, S.F. Zhang, D. Zhao, X.F. Jiang, C.L. Zhang, Y. Wang, Z.J. Li, N. Li, S. Xiao, W.C.H. Choy, A.K.Y. Jen, S.F. Yang, Z.L. Zhu, Highly Efficient Flexible Perovskite Solar Cells through Pentylammonium Acetate Modification with Certified Efficiency of 23.35%, *Adv. Mater.* (2023) 8.
- [6] C.X. Gong, L. Zhang, X.C. Meng, Z. Xing, L. Rao, H.Y. Wang, Z.Q. Huang, L.C. Tan, T. Hu, X.T. Hu, Y.W. Chen, A non-wetting and conductive polyethylene dioxythiophene hole transport layer for scalable and flexible perovskite solar cells, *Sci. China-Chem.* 64 (2021) 834–843.
- [7] N.Y. Ren, B.B. Chen, R.J. Li, P.Y. Wang, S. Mazumdar, B. Shi, C.J. Zhu, Y. Zhao, X. D. Zhang, Humidity-Resistant Flexible Perovskite Solar Cells with Over 20% Efficiency, *Sol. RRL* 5 (2021) 7.
- [8] J. Dou, Q.Z. Song, Y. Ma, H. Wang, G.Z. Yuan, X.Y. Wei, X.X. Niu, S. Ma, X.Y. Yang, J. Dou, S.C. Liu, H.P. Zhou, C. Zhu, Y.H. Chen, Y.J. Li, Y. Bai, Q. Chen, Improved interfacial adhesion for stable flexible inverted perovskite solar cells, *J. Energy Chem.* 76 (2023) 288–294.
- [9] W.B. Deng, F.M. Li, J.Y. Li, M. Wang, Y.C. Hu, M.Z. Liu, Anti-solvent free fabrication of FA-Based perovskite at low temperature towards to high performance flexible perovskite solar cells, *Nano Energy* 70 (2020) 8.
- [10] S. Song, E.Y. Park, B.S. Ma, D.J. Kim, H.H. Park, Y.Y. Kim, S.S. Shin, N.J. Jeon, T.-S. Kim, J. Seo, Selective Defect Passivation and Topographical Control of 4-Dimethylaminopyridine at Grain Boundary for Efficient and Stable Planar Perovskite Solar Cells, *Advanced energy materials*, 11 (2021) 2003382.2003381-2003382.2003389.
- [11] T. Zhu, J. Su, F. Labat, I. Ciofini, T. Pauperté, Interfacial Engineering through Chloride-Functionalized Self-Assembled Monolayers for High-Performance Perovskite Solar Cells, *Advanced Science, Engineering and Medicine* 12 (2020) 744–752.
- [12] Q. Jiang, X. Zhang, J. You, SnO₂: A Wonderful Electron Transport Layer for Perovskite Solar Cells, *Small*, 14 (2018) 1801154-1801151-1801154-1801154.
- [13] E.H. Jung, B. Chen, K. Bertens, M. Vafaei, S. Teale, A. Proppe, Y. Hou, T. Zhu, C. Zheng, E.H. Sargent, Bifunctional Surface Engineering on SnO₂ Reduces Energy Loss in Perovskite Solar Cells, *ACS Energy Lett.* 5 (2020) 2796–2801.
- [14] J. Wu, Y. Cui, B. Yu, K. Liu, Y. Li, H. Li, J. Shi, H. Wu, Y. Luo, D. Li, Q. Meng, A Simple Way to Simultaneously Release the Interface Stress and Realize the Inner Encapsulation for Highly Efficient and Stable Perovskite Solar Cells, *Advanced functional materials*, 29 (2019) 1905336.1905331-1905336.1905311.
- [15] H.B. Mo, Q. Chen, D. Wang, D.X. Cheng, S. Maniyarasu, M.Z. Mokhtar, J. Jacobs, T. L. See, A.G. Thomas, R.J. Curry, L. Li, Z. Liu, Laser Processing of KBr-Modified SnO₂ for Efficient Rigid and Flexible Ambient-Processed Perovskite Solar Cells, *Sol. RRL* 6 (2022) 12.
- [16] D. Yang, R. Yang, K. Wang, C. Wu, X. Zhu, J. Feng, X. Ren, G. Fang, S. Priya, S. Liu, High efficiency planar-type perovskite solar cells with negligible hysteresis using EDTA-complexed SnO₂, *Nat. Commun.* 9 (2018) 3239.

- [17] Z. Zheng, F. Li, J. Gong, Y. Ma, J. Gu, X. Liu, S. Chen, M. Liu, Pre-Buried Additive for Cross-Layer Modification in Flexible Perovskite Solar Cells with Efficiency Exceeding 22%, *Adv. Mater.* 34 (2022) 2109879.
- [19] H. Zhang, H.F. Yao, J.X. Hou, J. Zhu, J.Q. Zhang, W.N. Li, R.N. Yu, B.W. Gao, S. Q. Zhang, J.H. Hou, Over 14% Efficiency in Organic Solar Cells Enabled by Chlorinated Nonfullerene Small-Molecule Acceptors, *Adv. Mater.* 30 (2018) 7.
- [20] H.F. Yao, J.W. Wang, Y. Xu, S.Q. Zhang, J.H. Hou, Recent Progress in Chlorinated Organic Photovoltaic Materials, *Accounts Chem. Res.* 53 (2020) 822–832.
- [21] Y. Lei, H.Y. Li, X.C. Liu, C.L. Qiu, H.Y. Wang, X.L. Gong, Y.F. Ni, R.Z. Feng, J. Q. Peng, Y. Liu, H.M. Li, Hydrogen-iodide bonding between glycine and perovskite greatly improve moisture stability for binary PSCs, *Org. Electron.* 108 (2022) 9.
- [22] J. Zhuang, P. Mao, Y. Luan, N. Chen, X. Cao, G. Niu, F. Jia, F. Wang, S. Cao, J. Wang, Rubidium Fluoride Modified SnO₂ for Planar n-i-p Perovskite Solar Cells, *Advanced functional materials*, 31 (2021) 2010385.2010381-2010385.2010388.
- [23] X. Guo, J. Du, Z. Lin, J. Su, L. Feng, J. Zhang, Y. Hao, J. Chang, Enhanced efficiency and stability of planar perovskite solar cells using SnO₂:InCl₃ electron transport layer through synergistic doping and passivation approaches, *Chemical engineering journal*, 407 (2021) 127997-127991-127997-127998.
- [24] G.Z. Liu, H.Y. Zheng, H.F. Xu, L.Y. Zhang, X.X. Xu, S.D. Xu, X. Pan, Interface passivation treatment by halogenated low-dimensional perovskites for high-performance and stable perovskite photovoltaics, *Nano Energy* 73 (2020) 9.
- [25] J.H. Ren, T.H. Liu, B.C. He, G.B. Wu, H. Gu, B.Z. Wang, J.L. Li, Y.L. Mao, S. Chen, G.C. Xing, Passivating Defects at the Bottom Interface of Perovskite by Ethylammonium to Improve the Performance of Perovskite Solar Cells, *Small* 18 (2022) 8.
- [26] P.Y. Xu, H.Y. He, J.J. Ding, P. Wang, H.J. Piao, J.H. Bao, W.H. Zhang, X.P. Wu, L. B. Xu, P. Lin, X.G. Yu, C. Cui, Simultaneous Passivation of the SnO₂/Perovskite Interface and Perovskite Absorber Layer in Perovskite Solar Cells Using KF Surface Treatment, *ACS Appl. Energ. Mater.* 4 (2021) 10921–10930.
- [27] Y. Dong, W.J. Shen, W. Dong, C. Bai, J. Zhao, Y.C. Zhou, F.Z. Huang, Y.B. Cheng, J. Zhong, Chlorobenzenesulfonic Potassium Salts as the Efficient Multifunctional Passivator for the Buried Interface in Regular Perovskite Solar Cells, *Adv. Energy Mater.* 12 (2022) 12.
- [28] Y. Sun, J. Zhang, H. Yu, J. Wang, C. Huang, J. Huang, Mechanism of bifunctional p-amino benzenesulfonic acid modified interface in perovskite solar cells, *Chem. Eng. J.* 420 (2021), 129579.
- [29] A.S. Lin, P.N. Liu, S. Pratik, Z.K. Yang, T. Rawat, T.Y. Tseng, RRAM Compact Modeling Using Physics and Machine Learning Hybridization, *IEEE Trans. Electron Devices* 69 (2022) 1835–1841.
- [30] H. Bi, X. Zuo, B.B. Liu, D.M. He, L. Bai, W.Q. Wang, X. Li, Z.Y. Xiao, K. Sun, Q. L. Song, Z.G. Zang, J.Z. Chen, Multifunctional organic ammonium salt-modified SnO₂ nanoparticles toward efficient and stable planar perovskite solar cells, *J. Mater. Chem. A* 9 (2021) 3940–3951.
- [31] H. Bi, B.B. Liu, D.M. He, L. Bai, W.Q. Wang, Z.G. Zang, J.Z. Chen, Interfacial defect passivation and stress release by multifunctional KPF6 modification for planar perovskite solar cells with enhanced efficiency and stability, *Chem. Eng. J.* 418 (2021) 10.
- [32] Z.W. Ma, R.N. Yu, Z.Y. Xu, G.Z. Wu, H.Z. Gao, R.Y. Wang, Y.S. Gong, J. Yang, Z. A. Tan, Crosslinkable and Chelatable Organic Ligand Enables Interfaces and Grains Collaborative Passivation for Efficient and Stable Perovskite Solar Cells, *Small* 18 (2022) 11.
- [33] D. Yang, R.X. Yang, K. Wang, C.C. Wu, X.J. Zhu, J.S. Feng, X.D. Ren, G.J. Fang, S. Priya, S.Z. Liu, High efficiency planar-type perovskite solar cells with negligible hysteresis using EDTA-complexed SnO₂, *Nat. Commun.* 9 (2018) 11.
- [34] X. Peng, S.S. Zhao, R.N. Zhou, X.L. Gong, H.X. Luo, Y.K. Ouyang, X.C. Liu, H.M. Li, H.Y. Wang, J. Zhuang, A Versatile Organic Salt Modified SnO₂ Electron Transport Layer for High-Performance Perovskite Solar Cells, *Adv. Mater. Interfaces* 8 (2021) 8.
- [35] H. Wang, F.B. Li, P. Wang, R. Sun, W. Ma, M.T. Chen, W.Q. Miao, D. Liu, T. Wang, Chlorinated Fullerene Dimers for Interfacial Engineering Toward Stable Planar Perovskite Solar Cells with 22.3% Efficiency, *Adv. Energy Mater.* 10 (2020) 9.
- [36] K.L. Wang, M. Li, Y.H. Lou, J. Chen, Y.R. Shi, C.H. Chen, Y.H. Zhou, Z.K. Wang, L. S. Liao, Aniline Sulfonic Acid Induced Uniform Perovskite Film for Large-Scale Photovoltaics, *Adv. Energy Mater.* 13 (2023) 8.
- [37] H.Y. Wang, Y.K. Ouyang, W.J. Zou, X.C. Liu, H.M. Li, R.N. Zhou, X. Peng, X. L. Gong, Enhanced Activation Energy Released by Coordination of Bifunctional Lewis Base D-Tryptophan for Highly Efficient and Stable Perovskite Solar Cells, *ACS Appl. Mater. Interfaces* 13 (2021) 58458–58466.
- [38] Z.G. Xiao, Q.F. Dong, C. Bi, Y.C. Shao, Y.B. Yuan, J.S. Huang, Solvent Annealing of Perovskite-Induced Crystal Growth for Photovoltaic-Device Efficiency Enhancement, *Adv. Mater.* 26 (2014) 6503–6509.
- [39] S.M. Yang, H. Zhao, Y. Han, C.Y. Duan, Z.K. Liu, S.Z. Liu, Europium and Acetate Co-doping Strategy for Developing Stable and Efficient CsPbI₂Br Perovskite Solar Cells, *Small* 15 (2019) 9.
- [40] P.Y. Liu, N. Han, W. Wang, R. Ran, W. Zhou, Z.P. Shao, High-Quality Ruddlesden-Popper Perovskite Film Formation for High-Performance Perovskite Solar Cells, *Adv. Mater.* 33 (2021) 40.
- [41] N.X. Li, S.X. Tao, Y.H. Chen, X.X. Niu, C.K. Onwudinanti, C. Hu, Z.W. Qiu, Z.Q. Xu, G.H.J. Zheng, L.G. Wang, Y. Zhang, L. Li, H.F. Liu, Y.Z. Lun, J.W. Hong, X.Y. Wang, Y.Q. Liu, H.P. Xie, Y.L. Gao, Y. Bai, S.H. Yang, G. Brocks, Q. Chen, H.P. Zhou, Cation and anion immobilization through chemical bonding enhancement with fluorides for stable halide perovskite solar cells, *Nat. Energy* 4 (2019) 408–415.
- [42] D. Yang, X. Zhou, R.X. Yang, Z. Yang, W. Yu, X.L. Wang, C. Li, S.Z. Liu, R.P. H. Chang, Surface optimization to eliminate hysteresis for record efficiency planar perovskite solar cells, *Energ. Environ. Sci.* 9 (2016) 3071–3078.
- [43] A.A.B. Baloch, F.H. Alharbi, G. Grancini, M.I. Hossain, M.K. Nazeeruddin, N. Tabet, Analysis of Photocarrier Dynamics at Interfaces in Perovskite Solar Cells by Time-Resolved Photoluminescence, *J. Phys. Chem. C* 122 (2018) 26805–26815.
- [44] P.Y. Wang, Q. Jiang, Y. Zhao, Y. Chen, Z.M. Chu, X.W. Zhang, Y.Q. Zhou, J.B. You, Synergistic improvement of perovskite film quality for efficient solar cells via multiple chloride salt additives, *Sci. Bull.* 63 (2018) 726–731.
- [45] J.H. Chen, L.J. Zuo, Y.Z. Zhang, X.M. Lian, W.F. Fu, J.L. Yan, J. Li, G. Wu, C.Z. Li, H.Z. Chen, High-Performance Thickness Insensitive Perovskite Solar Cells with Enhanced Moisture Stability, *Adv. Energy Mater.* 8 (2018) 10.
- [46] M. Dehghanipour, A. Behjat, A.M.H. Shabani, M.A. Haddad, Toward desirable 2D/3D hybrid perovskite films for solar cell application with additive engineering approach, *J. Mater. Sci.-Mater. Electron.* 33 (2022) 12953–12964.
- [47] S. Jia, J.F. Wang, L. Zhu, Enhancing the photovoltaic performance of perovskite solar cells by potassium ions doping, *J. Mater. Sci. Mater. Electron.* 30 (2019) 2057–2066.